Three-dimensional volcanic aerosol dispersal: A comparison between Multiangle Imaging Spectroradiometer (MISR) data and numerical simulations

S. Scollo,[1] A. Folch,[2] M. Coltelli,[1] and V. J. Realmuto[3]

Received 5 September 2009; revised 18 May 2010; accepted 21 May 2010; published 21 December 2010.

[1] The three-dimensional reconstruction of volcanic plumes is a central goal to enhance our understanding on dispersal processes. In this paper we use data from the Multiangle Imaging Spectroradiometer (MISR) on board NASA's Terra spacecraft combined with a stereo matching retrieval procedure. We show the potential of MISR in capturing important features of volcanic plumes like column height, optical depth, type, and shape of the finest particles of two highly explosive eruptions occurring on Mount Etna in 2001 and 2002. This work tests how tephra dispersal models reconstruct the 3-D shape of volcanic clouds. We compare MISR data with FALL3D, an Eulerian model for the transport and deposition of volcanic ash and aerosols coupled with the Weather Research and Forecasting mesoscale meteorological model. Agreement between simulations and MISR data is good regarding both events, although it could be improved by increasing the accuracy of the meteorological data, a better constraint on volcanological input parameters like the height of the eruptive column and improving our understanding of processes such as aggregation phenomena and volcanic cloud microphysics.

Citation: Scollo, S., A. Folch, M. Coltelli, and V. J. Realmuto (2010), Three-dimensional volcanic aerosol dispersal: A comparison between Multiangle Imaging Spectroradiometer (MISR) data and numerical simulations, *J. Geophys. Res.*, *115*, D24210, doi:10.1029/2009JD013162.

1. Introduction

[2] Explosive volcanic eruptions can eject large quantities of particles that remain airborne in the atmosphere for long periods of time and form volcanic clouds [*Rose et al.*, 2001]. Because of their impact on air traffic [e.g., *Prata*, 2009], a crucial aspect in terms of prevention and forecasting is the prompt assessment of the column height and plume extent. Column height serves to evaluate mass eruption rate that provides an indication of eruption intensity [*Pyle*, 2000], identify the area potentially affected by ash fallout [e.g., *Carey and Sparks*, 1986], and initialize tephra dispersal models [*Mastin et al.*, 2009]. In turn the extent of the volcanic cloud delimits the current hazardous area and may be used to infer important characteristics of the eruption using backward trajectory models. Cloud height estimations can be obtained from observations on the ground or by plane [e.g., *Andronico et al.*, 2008], radar measurements [e.g., *Lacasse et al.*, 2004], or satellite retrievals [e.g., *Prata and Grant*, 2001]. However, important discrepancies may occur among different observational methods [e.g., *Tupper and Wunderman*, 2009] as each methodology takes different phenomena into consideration [*Mastin et al.*, 2009].

[3] Volcanic Ash Advisory Centers (VAACs) and some Volcano Observatories make a combined use of satellite images and volcanic ash transport and dispersion models (VATDM) to detect and track ash clouds and forecast the regions affected by ash dispersal [e.g., *Peterson and Dean*, 2008; *Scollo et al.*, 2009]. Ash cloud forecasting can be hindered by a number of factors. It is clear that the reliability of a forecast depends on the accuracy of the VATDM inputs, which rely on other models (e.g., meteorological models) or on measurements and retrievals. For example, the presence of hydrometeors can prevent remote sensing instruments from detecting volcanic ash, and in some critical cases, hydrometeors completely mask the detection of ash clouds [*Prata et al.*, 2001]. On the other hand, accurate meteorological mesoscale forecasts may be unable to properly predict sudden wind variations and local circulation patterns in cases with complex topography and within the planetary boundary layer [*Folch et al.*, 2008a]. Furthermore, models simplify neglect some relevant physical aspects. For example, there is a low level of understanding of particle aggregation although this can have a dramatic effect on the dynamics of the cloud causing premature fallout of aggregates [*Durant et al.*, 2009] and formation of deposit secondary maxima [*Rose*, 1993]. Finally, it is worth noting that, as reflected in the post-event analysis of several explosive events, dispersal of tephra from a single eruption can be very complex

[1]Istituto Nazionale di Geofisica e Vulcanologia-Sezione Catania, Catania, Italy.
[2]Barcelona Supercomputing Center, Barcelona, Spain.
[3]Jet Propulsion Laboratory, California Institute of Technology, Pasadena, California, USA.

0148-0227/10/2009JD013162

Table 1. Vent Location, Main Characteristics of the Explosive Activity, Column Height, Total Mass, and Total Grain Size Distribution of 21–24 July 2001 and 27 October 2002 Eruptions

Year	Day/Month	Vent Location (m Above Sea Level)	Characteristics of the Explosive Activity	Column Height	Total Mass	Mode of Grain Size
2001	21–24 Jul	South flanks (from 3050 to 2100 m)	Violent strombolian activity, continuous ash emission, magma-water interaction, presence of aggregation	21 July: 3.5–4 km 22 July: 3.5–4 km 23 July: 5 km 24 July: 4.5 km	2.3×10^9 kg	2ϕ
2002	27 Oct	South flanks (from 2850 to 2600 m)	Lava fountaining, sustained eruption column, continuous ash emission	6 km	0.9×10^9 kg	0.5ϕ

[*Watt et al.*, 2009]. For example, eruptive style can alternate between weak and strong plumes causing different patterns of sedimentation [*Bonadonna and Phillips*, 2003; *Bonadonna et al.*, 2005] or the granulometry and composition of the erupted material [*Andronico et al.*, 2009] and mass eruption rate [*Scollo et al.*, 2007] may vary during the same eruption. The introduction of these variations in the models is very difficult and VATDM run with predefined or preliminary inputs that can differ substantially from those of the real eruption [*Folch et al.*, 2008b].

[4] To achieve a robust forecasting we must validate ash dispersal models properly. Validation is usually carried out in two dimensions by comparing numerical simulations with ground-based data collected after the eruptive event [*Bonadonna et al.*, 2002; *Scollo et al.*, 2008a] or with satellite images showing the extent of the ash cloud [e.g., *Barsotti et al.*, 2008]. Although relevant, two-dimensional vertically integrated data do not provide information on the extent and concentration of volcanic plumes at different heights. To date, measurements of 3-D plume properties are very scarce. An initial attempt was carried out by *Glaze et al.* [1999], who interpreted the brightness temperature variation of satellite images as a change of the surface normal inclination and extracted the eruption plume height at different points. In this sense, Multiangle Imaging Spectroradiometer (MISR) can provide a novel mechanism to extract three-dimensional information on volcanic aerosol, in this work indicating the finest component of volcanic ash (<10 μm).

[5] The goal of this paper is twofold. The first goal is to investigate the potentiality of MISR as a tool to reconstruct 3-D volcanic plume geometry. To this end, we use MISR data of two long-term Etna explosive eruptions occurring in 2001 and 2002. The second goal is to perform a 3-D comparison between these data and the FALL3D atmospheric dispersion model [*Costa et al.*, 2006; *Folch et al.*, 2008a]. The manuscript is arranged as follows. First, we overview the characteristics of the 2001 and 2002 Etna eruptions; second, we describe the modeling strategy including the MISR instrument, the retrieval procedure, and the FALL3D dispersal model. Finally, we present the results and discuss the ability and limitations of the MISR volcanic cloud observations.

2. The 2001 and 2002 Explosive Activity of Etna

[6] Mount Etna is one of the world's most active volcanoes, and together with Sakurajima in Japan, Popocatepetl in Mexico, and Soufriere Hills in Montserrat Island, it is among the volcanoes that most frequently disrupt airport operations. Over the last 20 years, the explosive activity of Etna has increased in frequency [*Branca and Del Carlo*, 2005]. The recent explosive eruptions of 2001 and 2002 produced volcanic plumes reaching heights up to 6 and 7 km (above sea level), respectively, and forced the shutdown of the Catania International Airport causing important economic damage at regional and national levels [e.g., *Guffanti et al.*, 2009].

[7] The 2001 Etna eruption began on 17 July 2001 from a complex system of fractures that opened on the NE and south flanks of the volcano [*Calvari et al.*, 2001]. The eruption was heralded by a set of seismic swarms. From 12 July (at 2144 UTC), 2645 earthquakes with magnitude $M_d \geq 1$ were recorded before the eruption onset, and the seismic activity continued throughout the eruptive period [*Patanè et al.*, 2003]. Lava flows were emitted on eastward the Valle del Bove and the southern slope of the volcano from seven fissures active over various periods of time [*Calvari et al.*, 2001]. The explosive activity, manifested as lava fountaining and strombolian activity, was mainly localized on the south flank. Two coalescent pit craters formed at 2570 m and produced the majority of the total ejected tephra between 19 July and 6 August [*Scollo et al.*, 2007]. This explosive activity had three distinct phases. The first phase (from 19 to 24 July) was dominated by phreatomagmatic activity and produced an eruption column of oscillating height, the second phase (from 25 to 30 July) was characterized by purely magmatic activity, and the last phase showed characteristics of vulcanian eruptions [*Taddeucci et al.*, 2004]. The resulting tephra deposit was bilobate in shape and entirely covered the SE flank of the volcano. *Scollo et al.* [2007] estimated a total erupted mass between 1.02×10^9 and 2.31×10^9 kg applying the exponential [*Pyle*, 1989] and power law [*Bonadonna and Houghton*, 2005] methods, respectively. The total grain size distribution was evaluated with the Voronoi tessellation method [*Bonadonna and Houghton*, 2005], showing a mode of 2ϕ (where ϕ is $-\log d$, being d the particle diameter in millimeters).

[8] The 2002 Etna eruption was one of the most spectacular events in the last years. The eruption began during the night of 26 October 2002 from two fissures opened on the NE and south flanks followed by a third fissure on the NE flank [*Andronico et al.*, 2005]. Like the 2001 event, a swarm of earthquakes preceded and accompanied the formation of eruptive fissures. The seismic network of the Istituto Nazionale di Geofisica e Vulcanologia, sezione di Catania (INGV-CT) recorded 862 earthquakes ($M_d \geq 1$) until the eruption ceased on 28 January 2003 [*Monaco et al.*,

2005]. Two lava flows formed along the NE fissures; the first was directed toward the NE and stopped after 2.8 km, the second was directed toward the east and stopped after 6.8 km on 3 November, destroying most of the Piano Provenzana tourist infrastructure. The eruptive activity at the south fissure lasted up to 28 January 2003 and was characterized by lava fountains forming high eruption columns, strombolian activity, and lava effusion directed toward the SW and south [*Andronico et al.*, 2005]. During the first days of activity, weak plumes rose up to 7 km in height [*Andronico et al.*, 2008]. Plumes were composite because different eruption columns from different vents merged to form a single plume or, more rarely, two plumes with different heights. Furthermore, the explosive activity produced lava fountains rising up to 600 m and magma jets appearing at a frequency of about 20–30 s [*Andronico et al.*, 2008]. After this sustained initial intensity, explosive activity diminished and formed very diluted or pulsating volcanic plumes. The maximum column height was about 7 km on 28 October; the mass and the total grain size distribution evaluated by the analysis of the deposit were $4.4 \pm 0.6 \times 10^{10}$ kg and 0.5ϕ, respectively [*Andronico et al.*, 2008]. Table 1 summarizes the main characteristics of 21–24 July 2001 and 27 October 2002.

3. Methods

3.1. MISR Data

3.1.1. Multiangle Imaging Spectroradiometer

[9] MISR is one of the instruments on board the Terra spacecraft, which is part of NASA's Earth Observing System [*Diner et al.*, 1998]. Terra follows a near-polar, 705 km Sun-synchronous orbit, crossing the equator at approximately 1030 local solar time. The swath width has been designed to be 360 km, so that full coverage of a latitude circle is achieved every 9 days at the equator and every 2 days near the poles. Nine separate cameras gather data in four spectral bands centered at 446.4, 557.5, 671.7, and 886.4 nm, corresponding to blue, green, red, and near-infrared wavelengths, respectively. One camera points toward the nadir and the other eight provide forward and aft view angles of 26.1°, 45.6°, 60.0°, and 70.5° displaced in a symmetrical arrangement with respect to the nadir camera. MISR has a global coverage of ±82° latitude and provides 275 m sampling in all bands of the nadir camera and in the red bands of the off-nadir cameras [*Muller et al.*, 2002], whereas the rest of channels have 1.1 km resolution [*Kahn et al.*, 2001; *Moroney et al.*, 2002; *Muller et al.*, 2002]. On-board calibration is performed monthly by multiple in-flight methodologies, and the uncertainty in absolute radiometric accuracy is estimated to be 3% [*Diner et al.*, 1998].

[10] Since 2000, MISR has provided a unique opportunity to study aerosol dispersal and shortwave radiative properties [*Diner et al.*, 2001]. MISR products incorporate a set of aerosol models that are considered to be representative of different aerosols present in the Earth's atmosphere [*Diner et al.*, 2005]. MISR distinguishes different types of clouds, land surface cover, and aerosol [e.g., *Di Girolamo and Wilson*, 2003; *Kalashnikova and Kahn*, 2006]. The aerosol retrieval is based on some assumptions and physical constraints [*Martonchik et al.*, 1998]: aerosol distribution is assumed horizontally homogeneous within 17.6 × 17.6 km region at the surface, and retrievals are carried out by comparing observed radiances with precomputed model radiances obtained from predefined aerosol mixtures (combinations of up to three individual aerosol components). The retrievals are based on the best fit between the observed and model spectra, as determined by χ^2 statistical tests. Aerosols considered in the MISR retrieval are sea spray (salt), sulfate/nitrate particles, mineral dust, and biomass burning particles [*Kahn et al.*, 2001; *Kalashnikova and Kahn*, 2006].

3.1.2. MISR Interactive Explorer Software

[11] For the purposes of this study, MISR data were analyzed using a program named MINX (MISR interactive explorer) that was designed to analyze smoke, volcanic, and dust plume heights [*Nelson et al.*, 2008]. MINX provides height and wind retrievals at higher resolution and often with greater precision than the standard MISR retrievals. A stereo matching technique compares red band data between each of six off-nadir cameras and the nadir or reference camera. The technique matches similar features at a scale of a few hundred meters to determine the apparent offsets, or disparities, in the position of these features in the multiangle imagery and then uses this information to compute feature height and the wind vectors in the cross-track and along-track directions at these heights. Because the motion direction is provided by the user, when a plume is digitized, the number of unknowns is reduced from three to two: plume height and the ratio of speed across to speed along-track. The vertical precision of this method can be a few hundred meters under good conditions (D. Nelson, personal communication, 2009). However, various factors such as cloud contamination, plume turbulence, and low optical thickness can degrade retrieval quality. In particular, retrievals are difficult when the direction of plume motion is parallel to the along-track direction of the spacecraft. Furthermore, wind is an important factor in the stereo matching process because the disparity can be a combination of the parallax, due strictly to geometry, and an actual shift in a cloud location due to winds [*Martonchik et al.*, 2009]. MINX retrieves the wind vector at a specific height known as the "no wind-corrected heights" and, for the wind retrieval that pass a quality assessment, derives a "wind-corrected height." For this reason the no wind-corrected heights are less accurate, but they have a more complete coverage (see details in https://www.openchannelsoftware.com/projects/MINX). In addition to height, MINX generates estimates of aerosol optical thickness or aerosol optical depth (AOD) (i.e., the extinction coefficient integrated over a vertical column of unit cross section from the Earth's surface to the top of the atmosphere), Angstrom exponent (Å) (i.e., exponent of power law representation of extinction versus the wavelength, usually inversely related to the average size of the aerosol particles), and single scattering albedo (SSA) [*Diner et al.*, 1998] (the ratio of scattering efficiency to total light extinction). Finally, MINX gives the fraction of the green band optical depth value attributable to small ($<0.35\ \mu$m), medium ($0.35 < 0.7\ \mu$m), and large ($>0.7\ \mu$m) particle sizes and the fraction of the green band optical depth value attributable to spherical particles (τ fraction by particle size). It is important to note that the detection limit for particle size is strictly linked to the aerosol components available in the MISR retrieval algorithms. Aerosols are modeled using lognormal particle size distributions, characterized by the median radius and the standard deviation [*Kahn et al.*, 2001; *Kalashnikova and Kahn*, 2006], having larger particles with a mean radius of

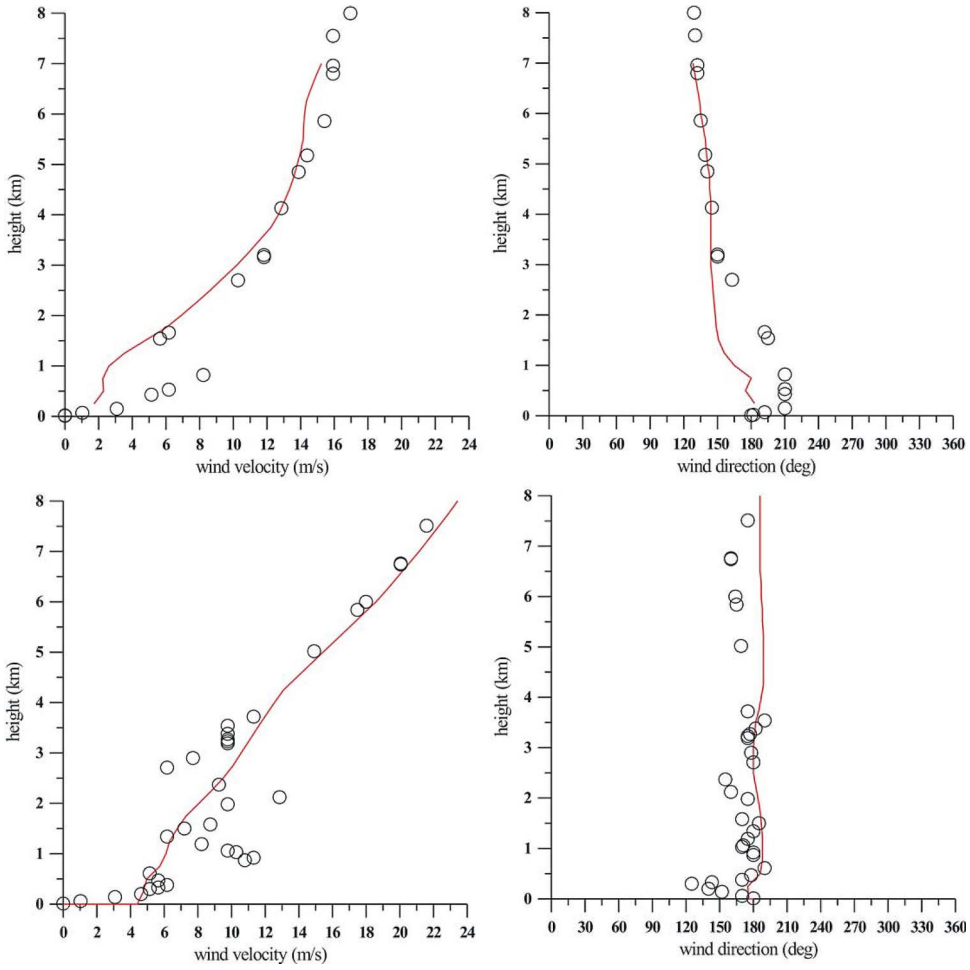

Figure 1. Comparison between sounding data at Trapani (dots) and WRF results (red line) during (top) 22 July 2001 at 0600 UTC and (bottom) 27 Oct 2002 at 06UTC.

2 μm and standard deviation of 2. Furthermore, MISR is more sensitive to particles between 0.05 and 2 μm in diameter [*Kahn et al.*, 1998] although studies have been carried out also including particles < 10 μm [e.g., *Jiang et al.*, 2007]. Here we assume 2.5–10 μm as the largest particle size detected by MISR. Hence, although volcanic clouds contain a mixture of gases (e.g., water, carbon dioxide, sulfur dioxide), aerosol (a dispersion of small (<10 μm) solid or liquid particles in a gas medium), and silicate ash particles (particles up to 2000 μm), in this study, we only consider the fraction of particles <10 μm. However, it is highlighted that the finer particles are able to reach major distances from the volcanic vent, and this size (<10 μm) is considered the most dangerous in terms of aviation hazard assessment.

3.2. Ash Cloud Modeling

[12] The modeling strategy is based on coupling a meteorological mesoscale model, a volcanic plume model based on the Buoyant Plume Theory (BPT) to describe the eruptive column [*Bursik*, 2001; *Carazzo et al.*, 2008], and the FALL3D atmospheric dispersion model [*Costa et al.*, 2006; *Folch et al.*, 2008a].

3.2.1. Weather Research and Forecasting

[13] The Weather Research and Forecasting (WRF) model is a fully compressible, Eulerian nonhydrostatic mesoscale meteorological model that solves equations of atmospheric motion [*Michalakes et al.*, 2005]. Here we use WRF to reproduce the meteorological conditions from 20 July 2001 at 1800 UTC to 26 July 2001 at 0000 UTC and from 26 October 2002 at 1200 UTC to 28 October 2002 at 0000 UTC. These time intervals cover an initial WRF spin-up period and the duration of the plume dispersal simulations. The WRF model was configured to integrate the primitive equations using the Advance Research WRF dynamics solver [*Skamarock et al.*, 2005] in three high-resolution-nested domains (horizontal resolutions of nests are 18, 6, and 2 km, respectively), with 40 vertical layers, and centered over western Sicily. We fixed the top pressure of the WRF model to 10 hPa. Initial and 6 hourly boundary conditions for WRF were obtained from the Global Forecast System reanalysis at 2.5° resolution. We tested the accuracy of the WRF results by comparing the simulated wind vertical profiles with atmospheric soundings at the nearest world meteorological station (Trapani, about 220 km west from Etna). Figure 1 shows simulated and measured vertical profiles of wind speed and direction at Trapani on 22 July 2001 (0600 UTC) and 27 October 2002 (0600 UTC). In general, there is a good agreement between soundings and WRF results except in the planetary boundary layer below 2–3 km, where differences of a few meters per second and from 10°

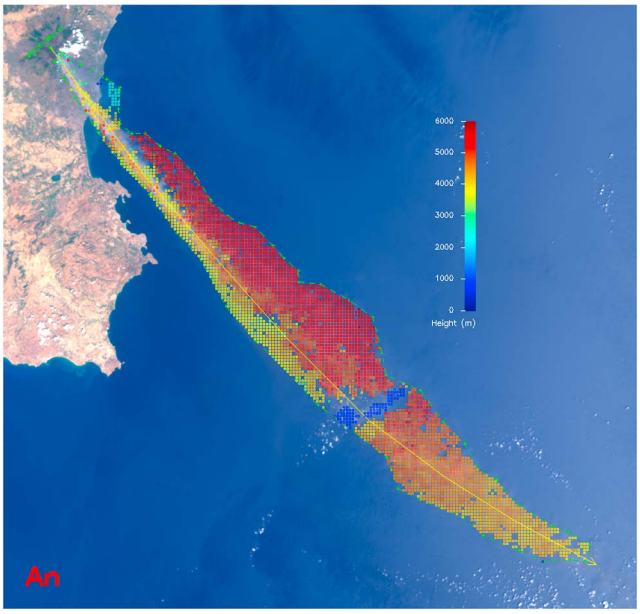

Figure 2. MISR nadir view of the Etna volcano plume during 22 July 2001 at 1000 UTC, orbit 8476, path 187. The image shows wind-corrected heights (color-coded), the digitized plume outline (green line), and the average wind direction (yellow line). The figure was generated by MINX software.

to 30° are typically observed for wind velocities and wind directions, respectively.

3.2.2. FALL3D

[14] FALL3D [*Costa et al.*, 2006; *Folch et al.*, 2008a] is an Eulerian model that simulates the transport and deposition of volcanic ash. The model solves the advection-diffusion-sedimentation equation with turbulent diffusion given by gradient transport theory, a class-dependent particle terminal velocity model, and a time-dependent three-dimensional wind field furnished by global or mesoscale meteorological models like WRF. The model accounts for terrain effects and can deal simultaneously with a wide spectrum of particle sizes (from lapilli to very fine ash) and gas components (e.g., H_2O or SO_2). The main volcanological model inputs are mass eruption rate, total grain size distribution, height, and shape of eruption column. FALL3D has already been validated against ground data and/or Moderate Resolution Imaging Spectroradiometer (MODIS) images for the 2001 Etna eruption [*Costa et al.*, 2006] and for other eruptions [e.g., *Folch et al.*, 2008b]. The model runs daily at INGV-CT and the results are used to forecast plume dispersal during Etna explosive events [*Scollo et al.*, 2009]. Here we couple the FALL3D model with the hourly WRF meteorological fields following an off-line strategy to simulate the 22 July 2001 and 27 October 2002 eruptive events.

4. Results

[15] The chemical, physical, and optical characteristics of volcanic aerosols erupted during 2001 and 2002 Etna eruptions have been characterized using both ground-based and remote sensing systems [e.g., *Pappalardo et al.*, 2004; *Wang et al.*, 2008; *Filizzola et al.*, 2007]. However, the MISR data acquired over Etna during these eruptions gives an opportunity to reconstruct the volcanic plume geometry and compare MISR stereoscopic retrievals with numerical simulations. It is important to state that the inputs for the dispersal model have been obtained from field studies and observations that are absolutely independent of MISR retrievals.

4.1. MISR Retrievals

[16] During the first phase of 2001 Etna eruption, MISR detected the Etna volcanic plume on 22 July 2001 at about 1000 UTC. Stereoscopic wind-corrected heights are shown in Figure 2 and indicate a narrow SE-directed plume extending for more than 200 km downwind. The image reveals the presence of volcanic aerosol at different heights along the volcanic plume, with higher and lower heights to the right and left of the main axis, respectively. These differences, as retrieved by MINX, may be attributed to variations of wind direction as a function of the height.

[17] Figure 3 shows wind-corrected heights as a function of the distance from the vent. The detected top heights of the volcanic plume are around 6 km at about 70 and 150 km away from the vent. Moreover, the figure shows a bent-over shape of the plume near the source because of wind action and an increase of volcanic particles in the lower part of the plume. This could be explained not only by the emission of ash at different heights along the eruptive column but also as a result of an abrupt decrease in particle settling velocity occurring at the plume-air interface [*Carey*, 1997]. The latter causes the formation of fingers, which were observed during 2001 and 2002 Mount Etna eruptions. Figures 2 and 3 highlight the difficulties of MISR in detecting particles at about 25 and 175 km from the vent due to the presence of clouds.

[18] Figure 4 shows the stereo height histograms of the volcanic plumes at four selected regions located at 100, 150, 200, and 250 km from the volcanic vent. The retrieved plume heights are between 5 and 5.5 km in the first region (100 km from the vent) remaining constant in the second region (150 km from the vent). However, the heights decrease

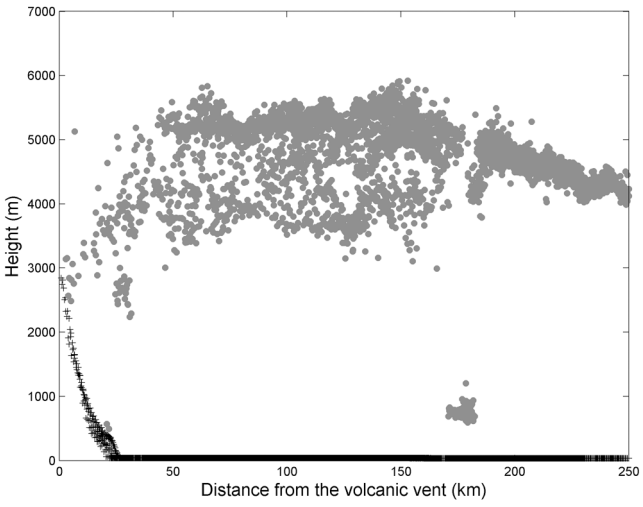

Figure 3. MISR wind-corrected heights as a function of the vent distance during 22 July 2001 at 1000 UTC. Gray points indicate MISR data; black crosses represent topography.

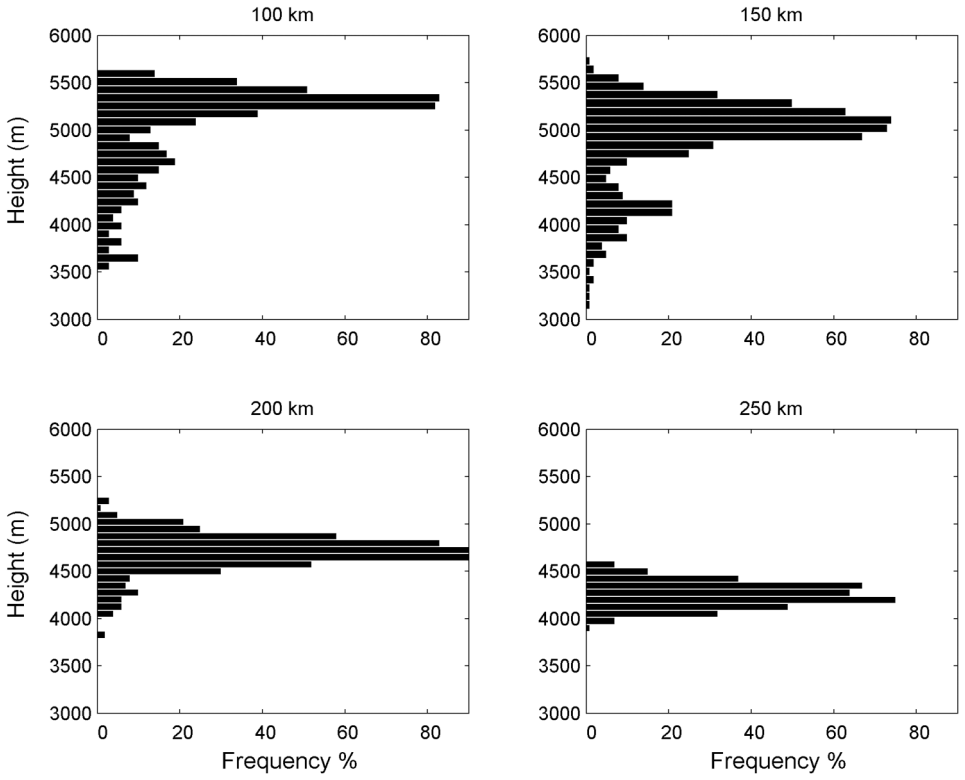

Figure 4. MISR height histograms of the 22 July 2001 volcanic plume at four selected regions. Regions are located along the dispersal axes at 100, 150, 200, and 250 km from the volcanic vent, respectively. The vertical bin size is 250 m, and the horizontal pixel resolution is 1.1 km.

to 4.5–5 km and 4–4.5 km in the third region (200 km from the vent) and in the fourth region (250 km from the vent), respectively. It follows that, according to the MINX retrieval, the height of the 2001 volcanic plume decreased approximately by 1 km along the main plume axes (SE) in about 250 km. Assuming a wind speed of 10 m/s (an average of the WRF results at that height), the resulting settling velocity should be of around 4 cm/s. This is consistent with the Stokes terminal velocity law for a sphere of diameter 20 μm and density of 2.5 g cm^{-3}, but it is 2 orders of magnitude larger than the theoretical value for a sphere of 2 μm in diameter.

[19] Finally, we also retrieved AOD between 0.07 and 0.27 with a mode equal to 0.12–0.13, a fraction of spherical particles of only 2%, a SSA_{558} value of 0.97 ± 0.2, and an Angstrom coefficient between 0.4 and 1.7.

[20] Figure 5 shows the imagery and the wind-corrected heights of the nadir camera of the volcanic plume retrieved on 27 October 2002 at 1000 UTC. The volcanic plume is directed toward SSE and covering a region wider than the 2001 Etna plume. Volcanic aerosols are above 4500 m toward the SSW and below 4500 m toward the SSE with more pronounced differences in height much than in the 2001 image (see Figure 2). In this case we interpret this as the result of multiple sources that formed a composite plume dispersed along two different axes.

[21] Figure 6 shows the wind-corrected heights as a function of the distance from the vent. The top plume height is approximately 6 km near the vent and reaches a maximum of 7 km at about 70 km downwind. This is in good agreement with the observations reported by *Andronico et al.* [2008]. It should be noted that the 27 October 2002 explosive activity was more intense than the 22 July 2001 activity, resulting in a volcanic plume having a slight bent-over shape due to the minor effect of wind on the eruption column.

[22] Histograms of MINX stereo heights at four regions located at 50, 150, 200, and 250 km from the vent are given in Figure 7. The region at 100 km from the vent was not considered because of few MINX data retrieved at this distance. The heights obtained by MINX are mainly between 5 and 5.5 km at the first region (50 km from the vent) and stay constant to 3–4 km in the next regions (from 150 to 250 km). This is inconsistent with the Stokes terminal velocity law for a sphere of diameter 10 μm and density of 2.5 g cm^{-3}.

[23] Finally, we retrieved AOD ranging between 0.025 and 0.95 with a mode between 0.39 and 0.4, a distribution composed mainly by medium and large size particles with a 3% of spherical particles, a value of SSA_{558} of 0.97 ± 0.2, and an Angstrom coefficient ranging between 0.04 and 1.3.

4.2. FALL3D Simulations

[24] We set the eruption source parameters (the date of onset, the duration of the eruption and run, the mass eruption rate, and the total gain size distribution) in FALL3D (Table 2). For the 2001 eruption, the modeling study focuses on the first phreatomagmatic phase, spanning the period from 21 July at 0000 UTC to 25 July at 0000 UTC. For simplicity, mass eruption rate was assumed to be constant for each day, with daily values ranging between 2.5 and 7.5 × 10^3 kg/s. The total erupted mass is 1.7 × 10^9 kg, a value very close to the 2.3 × 10^9 kg found by *Scollo et al.* [2007]. We considered

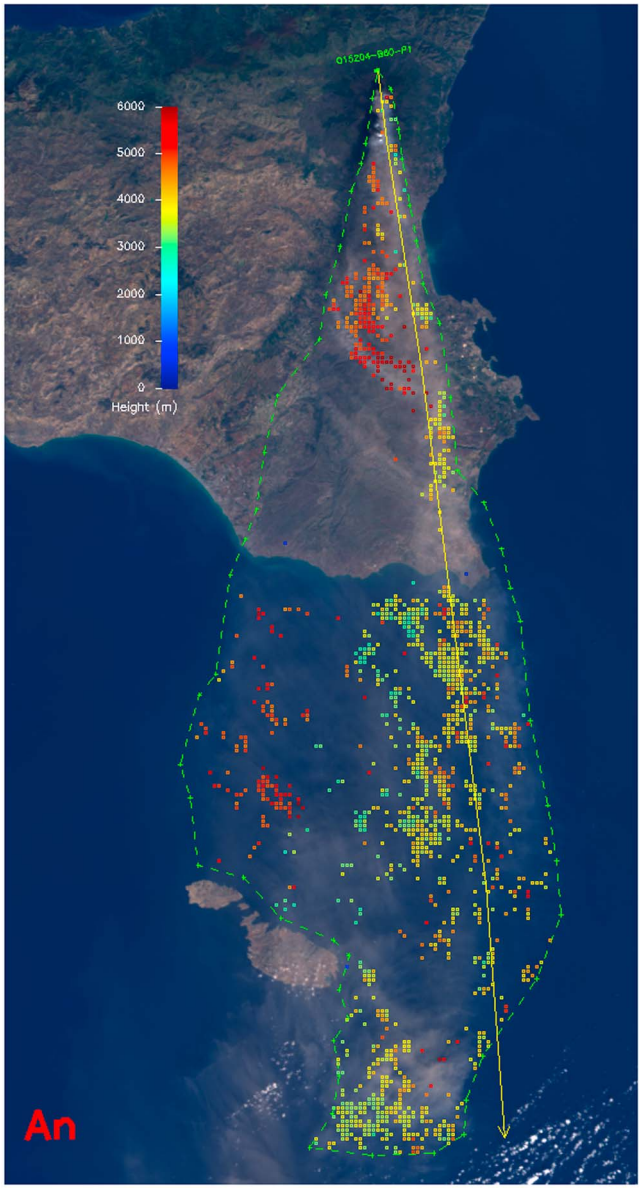

Figure 5. MISR nadir view of the Etna volcano plume during 27 October 2002 at 1000 UTC, orbit 15204, path 189. The image shows wind-corrected heights (color-coded), the digitized plume outline (green line), and the average wind direction (yellow line). The figure was generated by MINX software.

a 9 particle class Gaussian distribution ranging from -2ϕ (4 mm) to 7ϕ (8 μm) and peaked at 2ϕ (0.25 μm). The simulated fallout deposit is first emplaced toward the east on 21 July and then directed toward the SE on 22 July. The increase of the eruption intensity on 23 July (when the column reached the maximum height) caused a larger amount of tephra deposit on the SE flanks of the volcano (see Figure 8). The simulated deposit looks very similar in shape to that observed in the field [*Scollo et al.*, 2007, Figure 7] but off by a few degrees. We attribute this difference mainly to the errors in the simulated wind field direction, which are larger within the planetary boundary layer (PBL), where most of the transport occurred.

[25] For the 2002 case, we model the first day of the eruption (from 26 October 2100 UTC to 27 October 1000 UTC) and compare the results with field data collected on the ground [*Andronico et al.*, 2008]. On the basis of observations of explosive activity, we assigned a column height of 6000 m (±500 m), for which the BPT gives an averaged mass eruption rate of about 4×10^4 kg/s. As in the 2001 case, we also assume nine particle classes but with the Gaussian distribution peaked at 0.5ϕ (reflecting the magmatic nature of the 2002 event). The plume drifted SE at the beginning of the eruption and toward the SSW early in the morning of 27 October. The computed deposit (Figure 9) shows a good agreement with field data [*Andronico et al.*, 2008, Figure 4a].

4.3. Comparisons Between MISR Retrievals and FALL3D Simulations

[26] Figure 10 shows FALL3D concentration contours at 4000 and 5000 m superimposed on MINX results for 22 July 2001. To be consistent with the MISR aerosol size detection threshold, only the finest granulometric classes of FALL3D (<10 μm) are plotted. It is notable as all particles retrieved by MINX are inside the 10^{-4} g m^{-3} isoline. A difference of about 10° occurs at 5000 m between MINX results and the simulated plume dispersal axis. This discrepancy is likely caused by poor forecasting of the wind direction. Figure 11 compares MINX stereo height histograms of the plume at the four selected regions with normalized vertical concentration profiles simulated by FALL3D. Assuming that the number of particles per pixel is similar, the frequency histogram (i.e., the percentage of pixels with a given retrieved height) is proportional to the variation of concentration with height and hence can be directly compared to a normalized concentration. This gives information about the measured versus simulated volcanic cloud height, thickness, and shape. The differences are near the MISR resolution limit (500 m). Furthermore, the agreement between stereo height histograms and simulations improves on moving away from the volcanic vent (compare

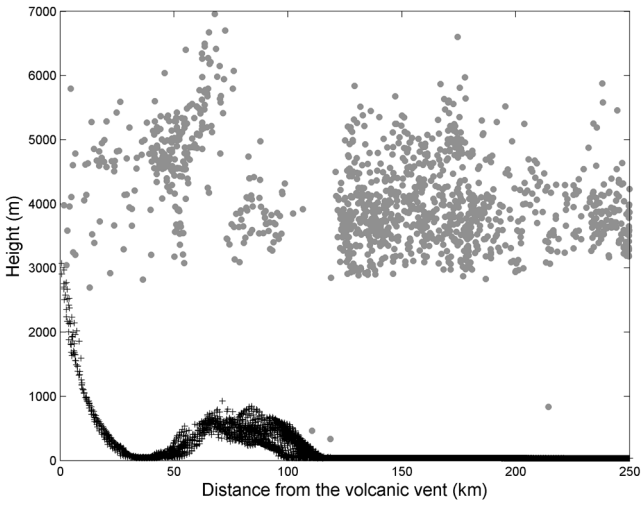

Figure 6. MISR wind-corrected heights as a function of the vent distance during 27 October 2002 at 1000 UTC. Gray points indicate MISR data; black crosses represent topography.

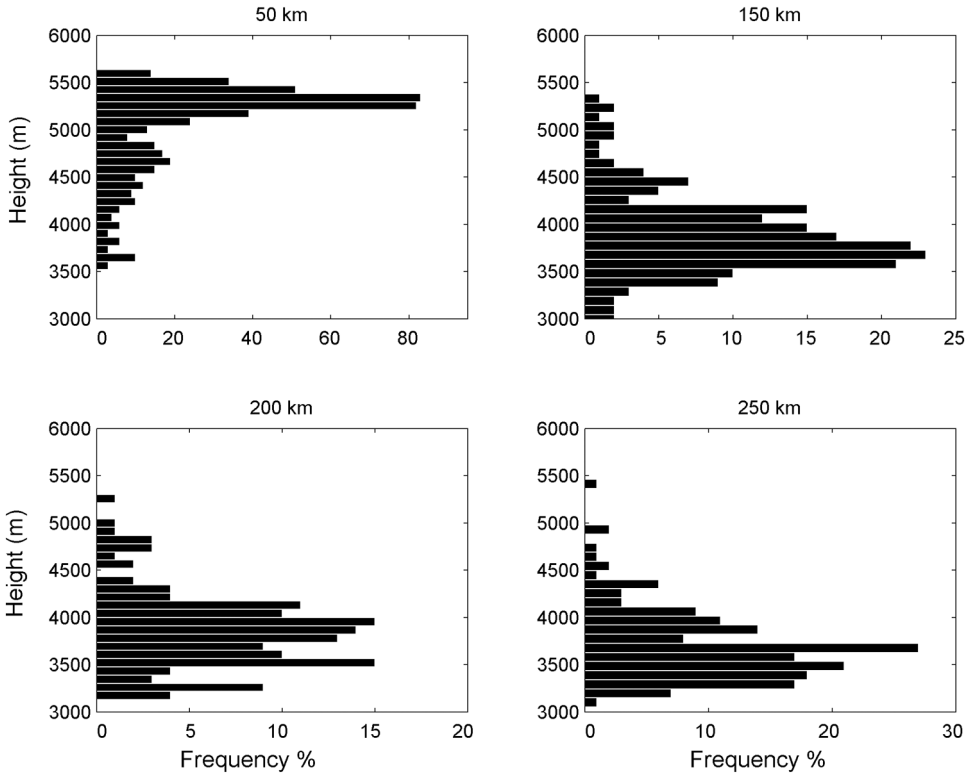

Figure 7. MISR height histograms of the 27 October 2002 volcanic plume at four selected regions. Regions are located along the dispersal axes, at 50, 150, 200, and 250 km from the volcanic vent, respectively. The figure was generated by MINX software.

regions at 50 and 200 km in Figure 11). It is highlighted that while MINX retrievals detected variations of volcanic ash heights at different distances from the vent, the vertical concentration profiles almost maintain the same height.

[27] Figure 12 compares simulated concentration contours with MINX retrieval at 4000 and 5000 m for 27 October 2002. All MINX results fall inside the 10^{-5} g m^{-3} isoline, and the differences in the direction of the plume are of about 15°. This difference is too large to be attributed only to inaccurate forecasting and reinforces the hypothesis of multiple sources (not contemplated by the model). Finally, Figure 13 shows the MINX stereo height histograms superimposed on simulated vertical concentration profiles for the selected regions, located at 50, 150, 200, and 250 km from the volcanic vent. As in the 2001 case, the variations of volcanic aerosol detected by MISR are not captured in the simulations. However, some of these variations could be attributed to ambiguity caused by the nearly along-track direction of plume motion.

5. Discussion

[28] The application of MISR to volcanic plumes seems to be promising. Indeed, volcanic plumes constitute a good target for space-based MISR instrumentation because the sources can remain active for long periods at fixed geographic locations and, moreover, the properties of volcanic fine ash are very distinctive from those of aerosols in the surrounding atmosphere [*Kahn et al.*, 2007]. Our opinion is that MISR may really become a very useful tool to study volcanic clouds and to mitigate its hazardous effects. Nowadays, volcanologists make use of predefined eruptive scenarios to evaluate the potential impacts of volcanic clouds and tephra fallout at regional level [*Mastin et al.*, 2009]. For

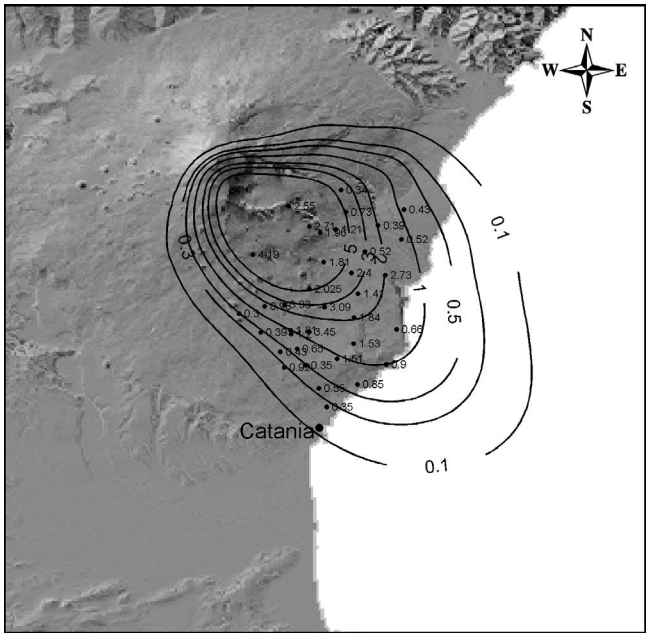

Figure 8. Deposit load (kg/m^2) computed by FALL3D and field data (kg/m^2) [*Scollo et al.*, 2007] for 21–24 July 2001.

Table 2. Date of Onset, Duration of the Eruption and Run, Mass Eruption Rate, and Total Grain Size Distribution Used in the Simulations of 21–24 July 2001 and 27 October 2002 Eruptions

Year	Date of Onset	Duration of the Eruption	Duration of the Run	Mass Eruption Rate (kg/s)	Total Grain Size Distribution
2001	21 Jul 0000 UTC	96 h	98 h	20 July: 2.5×10^3 kg/s 21 July: 2.5×10^3 kg/s 22 July: 7.5×10^3 kg/s 23 July: 7.5×10^3 kg/s	$2 \pm 1.5\phi$
2002	26 Oct 2100 UTC	24 h	26 h	4.0×10^4 kg/s	$0.5 \pm 1.5\phi$

example, everyday INGV-CT simulates three eruptive scenarios of Mount Etna similar to the 1998, 2001, and 2002 eruptions. The results are automatically delivered to the civil protection and aviation authorities to be eventually used as a first assessment of the volcanic ash plume impact [*Scollo et al.*, 2009]. In case of a real eruption, an important aspect in terms of mitigation is to discriminate, as quickly as possible, which of the simulated scenarios matches the actual eruption. Combined with other classical techniques, MISR could be an aid for this purpose. On the other hand, during an on-going explosive eruption, VATDM are also used by VAACs and volcano observatories to forecast trajectories of volcanic clouds and to estimate the expected short-term fallout. Regardless of the framework and the modeling strategy, the assessment of the eruptive parameters like column height, erupted mass, and the granulometric distribution of particles is important to improve the reliability of models. In fact, model sensitivity analysis [e.g., *Connor and Connor*, 2006; *Scollo et al.*, 2008b] has demonstrated that these parameters are among the most influent input data of tephra dispersal models. We argue that a syn-eruptive assimilation of MISR data into models would represent an important step forward to improve volcanic cloud forecasting.

[29] However, we point out that there are a number of limitations including such as MISR sensor views a relatively small portion of Earth at a single time and captures images of individual sites only about once per week [*Kahn et al.*, 2007]. It follows that it cannot be used as a "continuous" monitoring system as MODIS, or SEVIRI (Spin Enhanced Visible and Infrared Imager on board the Meteosat Second Generation geosynchronous satellite). MISR standard algorithm can fail in presence of clouds. Moreover, as pointed out by *Moroney et al.* [2002], the stereo matching retrieval algorithms can also fail in multilayered cloudy scenes, resulting in low-quality MISR's cloud-top height retrieval. Afterward, we describe the ability and limitation on volcanic cloud height and aerosol retrievals and on the modeling strategy used in this paper.

5.1. Ability and Limitation on Height Retrieval

[30] Today, several remote sensing or ground-based techniques are used to measure or to infer heights of volcanic plumes. Instruments like radar [e.g., *Lacasse et al.*, 2004] and lidar [*Sassen et al.*, 2007] are potentially suitable for this purpose. Other common strategies are to compare plume top infrared brightness temperatures with atmospheric profiles [e.g., *Holasek et al.*, 1996; *Sawada*, 1987, *Wen and Rose*, 1994] or to determine the height at which the ascent velocity of the volcanic plume equals the incident wind [e.g., *Tupper et al.*, 2004]. Alternatively, geometric techniques can also be used whenever the shadow of the plume is visible on the underlying Earth's surface [*Holasek et al.*, 1996; *Prata and Grant*, 2001] or even on meteorological clouds [*Oppenheimer*, 1998]. More recently, *Richards et al.* [2006] applied the MODIS CO_2 slicing algorithm (which uses five MODIS infrared bands) to measure eruption column heights of several explosive eruptions. Here we propose the space-based multiangle and multispectral MISR imaging as an alternative, novel, and powerful mechanism to study volcanic plumes. In fact, we found MISR data are in good agreement with observations collected during monitoring activities of INGV-CT. However, MINX retrieved heights and observations may differ because of a number of reasons. For example, differences could exist in case of oscillating columns if the precise instant of the MISR overpass does not coincide with the instant of the photo shot. Discrepancies could be due to the different dynamic regimes of the finer particles that may continue to rise because of buoyancy effects [*Bonadonna and Phillips*, 2003] resulting in MISR overestimating heights with respect to observations.

[31] The sensitivity and accuracy of the MISR stereo heights have already been validated against radar and lidar ground truth for meteorological clouds [*Moroney et al.*, 2002; *Naud et al.*, 2002, 2004, 2005]. MISR versus lidar comparisons [*Naud et al.*, 2004] has shown that differences in

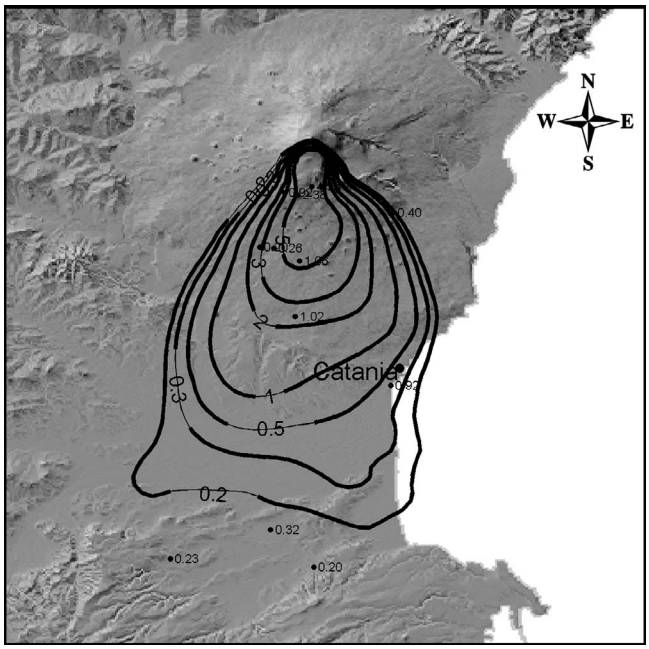

Figure 9. Deposit load (kg/m^2) computed by FALL3D and field data (kg/m^2) (courtesy of D. Andronico) for 27 October 2002.

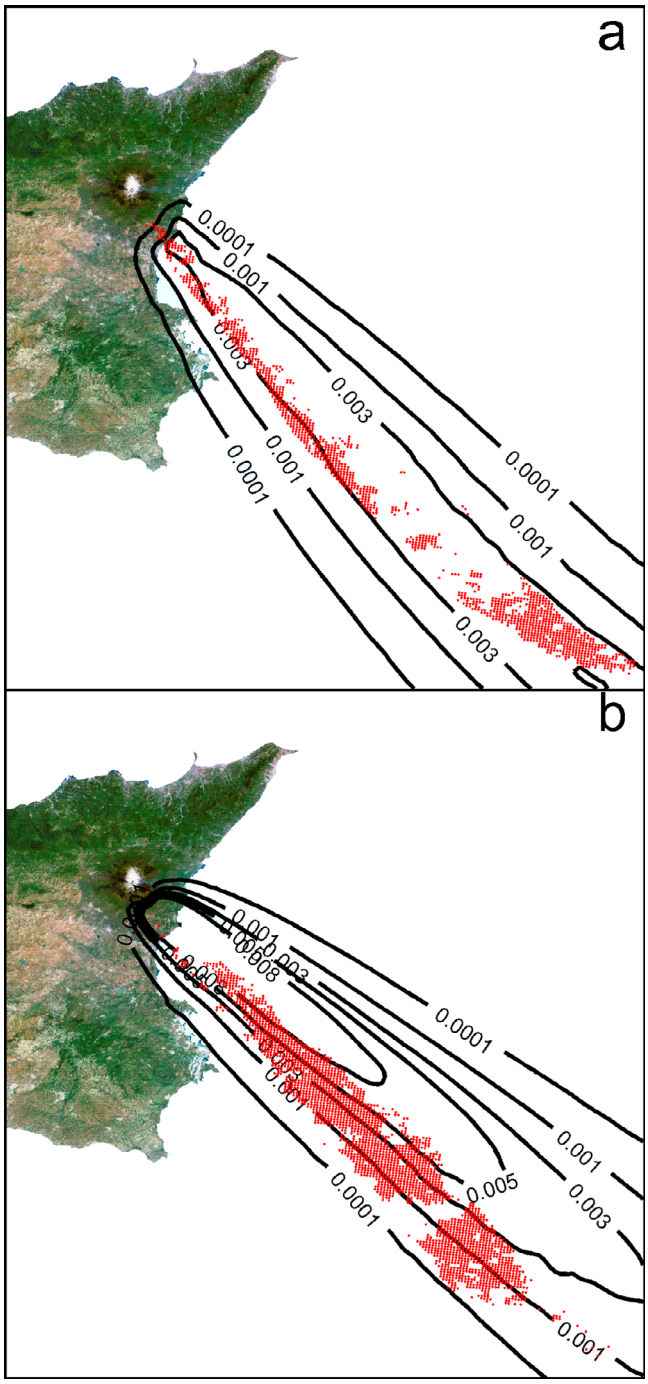

Figure 10. MISR data retrieved from 2001 Etna volcanic plume (dots) superimposed to ash (<10 μm) concentration contours in g/m^3 given by FALL3D: (a) cut at 4000 m and (b) cut at 5000 m.

measured heights range from 0.1 to a maximum of 0.4 km. We argue that similar results should be expected for volcanic plumes given the geometric nature of the retrieval method; that is to say, MISR and lidar should have a similar accuracy when they are applied to volcanic plumes. Thus, MISR data can be used in combination with other remote sensing (e.g., MODIS) or ground (e.g., lidar) techniques to evaluate eruption column heights with higher precision [*Genkova et al.*, 2007]. This opportunity could bring a great advancement on the quality of tephra dispersal forecasting.

5.2. Ability and Limitation on Aerosol Retrieval

[32] It is highlighted that MISR spectral range is sensitive mainly to aerosol particles of about 2.5 μm in diameter. In many volcanic eruptions, the mass fraction of fine ash with diameter lower than 2.5 μm is typically low, although this value varies widely depending on factors like magma composition or the occurrence of magma-water interaction [*Rose et al.*, 2000]. It is clear that the mass fraction of the volcanic plume viewed by MISR will increase with distance, when larger constituents are removed. However, on the base of the total grain size distribution carried out during 2001 and 2002–2003 Etna eruptions, MISR should detect about 1% of the total erupted volume/mass for both eruptions.

[33] Furthermore, *Kalashnikova et al.* [2005] demonstrated that MISR can be used to extract granulometric information of the finest plume components. Our analysis pointed out that the majority of particles detected by MISR belong to the medium (between 0.35 and 0.7 μm diameter) and large classes (larger than 0.7 μm) for 2001 and 2002 volcanic plumes, respectively. This is also consistent with the style of the explosive activity derived from the analysis of the deposit. In fact, the total grain size distribution of the 2001 eruption peaked at 2ϕ mainly due to magma-water interaction [*Scollo et al.*, 2007]. In contrast, the 2002 eruption was a purely magmatic type and generated a distribution of particles with a higher mean diameter, peaking at 0.5ϕ [*Andronico et al.*, 2008]. It is highlight that aerosol products, other than the aerosol optical thickness and plume height, are not validated globally [*Khan et al.*, 2007], and consequently, these values should be taken only qualitatively. If no wind-corrected heights are used, a greater number of points are detected by MISR. However, we found differences of only 8% and 30% using wind-corrected heights compared to no wind-corrected heights for 2001 and 2002 Etna eruptions, respectively.

5.3. Ability and Limitation on Modeling

[34] MISR has already been used to validate aerosol dispersal simulations [*Stenchikov et al.*, 2006], also in combination with Aerosol Robotic Network data [*Solomon et al.*, 2006; *Liu et al.*, 2004] and in this paper to validate tephra dispersal models. We found that ash concentration values up to 10^{-5} g/m^3 fit the MISR data for both 22 July 2001 and 27 October 2002 volcanic plumes. This threshold is in agreement with that used from VAAC of Montreal [*Witham et al.*, 2007] and could be used on hazard maps of models that forecast the ash dispersal in the atmosphere soon after the eruptive event. Furthermore, we pointed out that some discrepancies between MISR data and model results could be imputed to (1) inaccurate meteorological forecasting because of a lack of any meteorological and plume coupling [*Costa et al.*, 2006] and a less accuracy inside PBL where the complex topography of the volcano generates a more irregular wind field [*Barsotti and Neri*, 2008]; (2) uncertainties of the FALL3D modeled cloud heights that come from ground observations and are rounded considering the error of the observations (20%) and the vertical grid resolution (250 m);

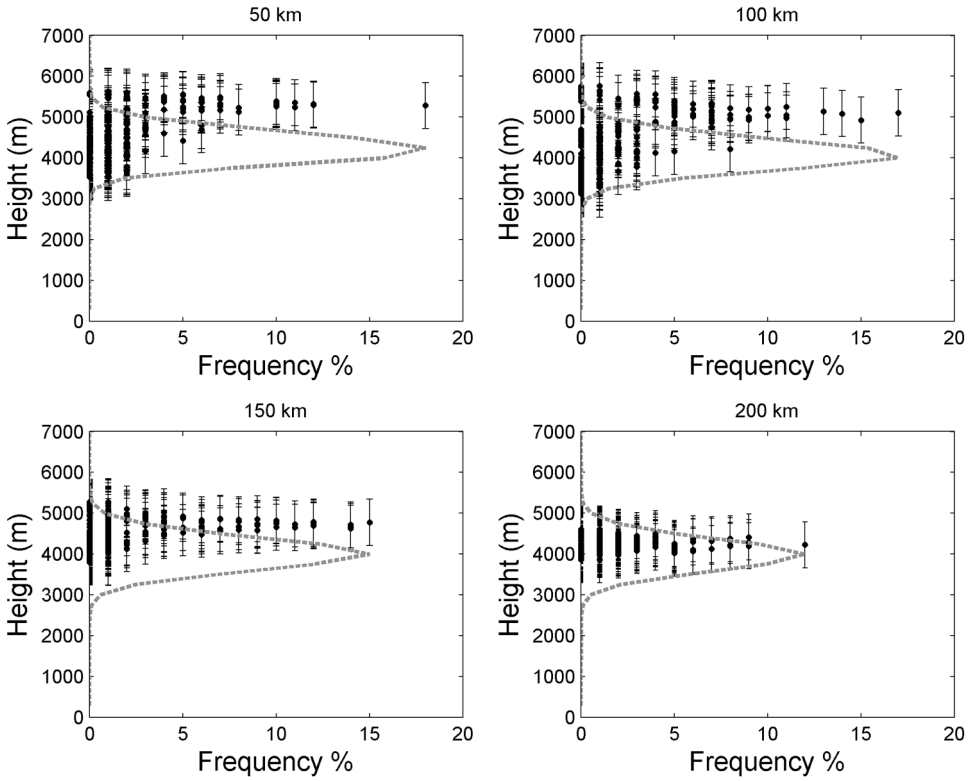

Figure 11. MISR heights (dots) and FALL3D normalized vertical concentration profiles (dashed lines) at the four selected regions along the 2001 plume dispersal axis.

(3) poorly understood processes such as particle buoyancy effects, aggregation processes, occurrence of particle loading and sublimation and evaporation of hydrometeors at the volcanic plume base that could verify into the plume [*Durant et al.*, 2009]; and (5) high variability of the eruptive activity that prove difficult to introduce into the modeling mainly because of a lack of "continuous" monitoring system of volcanic plumes.

6. Conclusions and Future Work

[35] This work has shown that MISR can detect some features of volcanic plumes, like height and shape of the

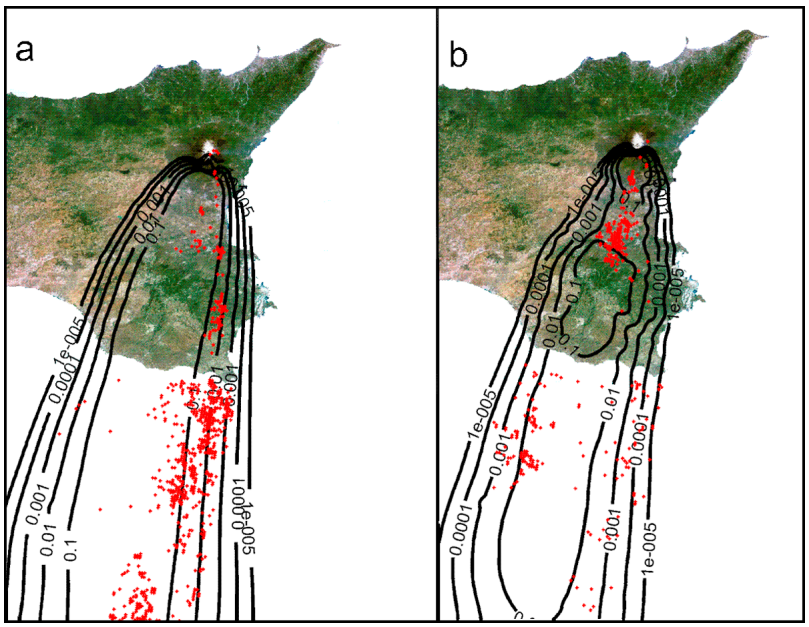

Figure 12. MISR data retrieved from 2002 Etna volcanic plume (dots) superimposed to ash (<10 μm) concentration contours in g/m^3 given by FALL3D: (a) cut at 4000 m and (b) cut at 5000 m.

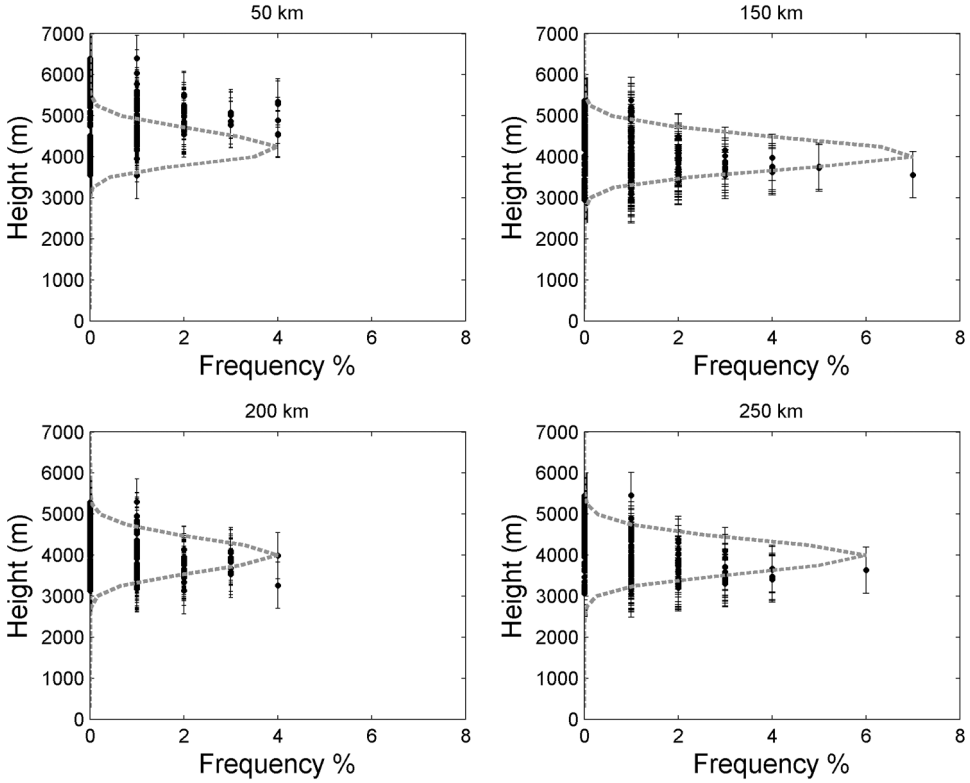

Figure 13. MISR heights (dots) and FALL3D normalized vertical concentration profiles (dashed lines) at the four selected regions along the 2002 plume dispersal axis.

eruption column, and relevant characteristics of the finest components. A 3-D comparison between MISR stereoscopic retrievals and numerical simulations using the FALL3D dispersal model indicates that the model is able to forecast the dispersion of ash properly providing that high-resolution meteorological data are available and that volcanological input parameters are well constrained. Column height is a key parameter, especially to model atmospheric concentration. In this sense, it is important to have ground and remote sensing techniques that can evaluate this parameter with high accuracy. Assimilation of MISR data into tephra dispersal models would improve its reliability and help to drastically reduce the threat to aviation.

[36] Future work includes the validations of MISR aerosol products using data collected by several instruments that detected Etna volcanic plumes during the last eruptions such as channel untracking photometer [e.g., *Watson and Oppenheimer*, 2000; 2001], airborne multispectral imaging spectrometer [e.g., *Spinetti et al.*, 2003; *Spinetti and Buongiorno*, 2007; *Remitti et al.*, 2006], lidar instruments [*Villani et al.*, 2006; *Fiorani et al.*, 2009], Moderate Resolution Imaging Spectroradiometer [*Corradini et al.*, 2008], Advanced Visible and Near-Infrared Radiometer [*Oppenheimer et al.*, 1998], aerosol spectrometers [*Allen et al.*, 2006]; space-born and ground-based instruments [e.g., *Zerefos et al.*, 2006]. In addition, tephra deposit could be evaluated by the MISR optical depth by applying techniques similar to those used by *Liu et al.* [2007] to predict ground-level $PM_{2.5}$ concentrations in St. Louis in Missouri (USA).

[37] **Acknowledgments.** The authors are grateful to D. Andronico and G. Bluth for their preliminary review of the paper. We thank M. Prestifilippo and M. Palano for providing plot base maps. The authors greatly thank the native speaker Stephen Conwey; Maria Carreras, and J.M. Baldasano, head of the BSC Earth Science Department, for supporting this work; David L. Nelson for his assistance in the analysis of the MISR data obtained by MINX and a review of the paper; the principal investigator David Diner and all the MISR team of NASA at Jet Propulsion Laboratory, California Institute of Technology, are sincerely thanked for their useful suggestions, encouragement to pursue this research, and support during the stay of one of the authors (Simona Scollo) at JPL. The MISR data used in this study were obtained from the NASA Langley Research Center Atmospheric Science Data Center. We greatly thank the editor Yinon Rudich, the reviewer Adam Durant, and two anonymous reviewers that improved the quality of the paper with their constructive suggestions. This work was funded by the FIRB project "Sviluppo Nuove Tecnologie per la Protezione e Difesa del Territorio dai Rischi Naturali" of Ministry of Universities and Research for one of the authors (S. Scollo), and by the HPC-Europa Transnational Access programme at the Barcelona Supercomputing Center (BSC). "Part of this research was performed at the Jet Propulsion Laboratory, California Institute of Technology, under a contract with the National Aeronautics and Space Administration".

References

Allen, A. G., T. A. Mather, A. J. S. McGonigle, A. Aiuppa, P. Delmelle, B. Davison, N. Bobrowski, C. Oppenheimer, D. M. Pyle, and S. Inguaggiato (2006), Sources, size distribution, and downwind grounding of aerosols from Mount Etna, *J. Geophys. Res.*, *111*, D10302, doi:10.1029/2005JD006015.

Andronico, D., et al. (2005), A multi-disciplinary study of the 2002–2003 Etna eruption: Insights for a complex plumbing system, *Bull. Volcanol.*, doi:10.1007/s00445-004-0372-8.

Andronico, D., S. Scollo, A. Cristaldi, and S. Caruso (2008), The 2002–2003 Etna explosive activity: Tephra dispersal and features of the deposit, *J. Geophys. Res.*, *113*, B04209, doi:10.1029/2007JB005126.

Andronico, D., S. Scollo, A. Cristalli, and F. Ferrari (2009), Monitoring ash emission episodes at Mt. Etna: The 16 November 2006 case study, *J. Volcanol. Geotherm. Res.*, *180*, 123–134.

Barsotti, S., A. Neri, and J. S. Scire (2008), The Vol-CALPUFF model for atmospheric ash dispersal: I Approach and physical formulation, *J. Geophys. Res.*, *113*, B03208, doi:10.1029/2006JB004623.

Barsotti, S., and A. Neri (2008), The VOL-CALPUFF model for atmospheric ash dispersal: 2. Application to the weak Mount Etna plume of July 2001, *J. Geophys. Res.*, *113*, B03209, doi:10.1029/2006JB004624.

Bonadonna, C., G. Macedonio, and R. S. J. Sparks (2002), Numerical modeling of tephra fallout associated with dome collapses and Vulcanian explosions: Application to hazard assessment on Montserrat, in *The eruption of Soufriere Hills Volcano, Montserrat, from 1995 to 1999*, edited by T. H. Druitt and B. P. Kokelaar, pp. 517–537, Geological Society, London, Memoir.

Bonadonna, C., and J. C. Phillips (2003), Sedimentation from strong volcanic plumes, *J. Geophys. Res.*, *108*(B7), 2340, doi:10.1029/2002JB002034.

Bonadonna, C., J. C. Phillips, and B. F. Houghton (2005), Modeling tephra sedimentation from a Ruapehu weak plume eruption, *J. Geophys. Res.*, *110*, B08209, doi:10.1029/2004JB003515.

Bonadonna, C., and B. F. Houghton (2005), Grain size distribution and volume of tephra fallout deposits, *Bull. Volcanol.*, *67*, 441–456, doi:10.1007/s00445-004-0386.

Branca, S., and P. Del Carlo (2005), Types of eruptions of Etna volcano A.D. 1670–2003: Implications for short-term eruptive behavior, *Bull. Volcanol.*, *67*, 732–742.

Bursik, M. (2001), Effect of wind on the rise height of volcanic plumes, *Geophys. Res. Lett.*, *18*, 3621–3624, doi:10.1029/2001GL013393.

Calvari, S., et al. (2001), Multidisciplinary approach yields insight into Mt Etna 2001 eruption, *Eos Trans.*, *82*, 653–656.

Carazzo, G., E. Kaminski, S. Tait (2008), On the dynamics of volcanic columns: A comparison of field data with a new model of negatively buoyant jets, *J. Volcanol. Geotherm. Res.*, *178*, 94–103.

Carey, S. N., and R. S. J. Sparks (1986), Quantitative models of the fallout and dispersal of tephra from volcanic eruption columns, *Bull. Volcanol.*, *48*, 109–125.

Carey, S. (1997), Influence of convective sedimentation on the formation of widespread tephra fall layers in the deep sea, *Geology*, *25*, 839–842.

Connor, L. G., and C. B. Connor (2006), Inversion is the key to dispersion: Understanding eruption dynamics by inverting tephra fallout, in *Statistics in Volcanology, Society for Industrial and Applied Mathematics*, *Special Publication of IAVCEI No. 1*, edited by H. Mader, S. Cole, and C. B. Connor, pp. 231–242, Geological Society, London.

Corradini, S., C. Spinetti, E. Carboni, C. Tirelli, M. F. Buongiorno, S. Pugnaghi, and G. Gangale (2008), Mt. Etna tropospheric ash retrieval and sensitivity analysis using Moderate Resolution Imaging Spectroradiometer measurements, *J. Appl. Remote Sens.*, *2*, doi:10.1117/1.3046674.

Costa, A., G. Macedonio, and A. Folch (2006), A three-dimensional Eulerian model for transport and deposition of volcanic ashes, *Earth Planet. Sci. Lett.*, *241*, 634–647.

Di Girolamo, L., and M. Wilson (2003), A first look at band-differenced angular signatures for cloud detection from MISR, *IEEE Trans. Geosci. Remote Sens.*, *41*(7), 1730–1734.

Diner, D. J., J. Beckert, T. Reilly, C. Bruegge, J. Conel, R. Kahn, J. Martonchik, T. Ackerman, R. Davies, S. Gerstl, et al. (1998), Multiangle Imaging Spectroradiometer (MISR) instrument description and experiment overview, *IEEE Trans. Geosci. Remote Sens.*, *36*, 1072–1087.

Diner, D. J., W. A Abdou, C. J. Bruegge, J. E. Conel, K. A. Crean, and B. J. Gaitley (2001), MISR aerosol optical depth retrievals over southern Africa during the SAFARI-2000 dry season campaign, *Geophys. Res. Lett.*, *28*(17), 3127–3130, doi:10.1029/2001GL013188.

Diner, D. J., B. H. Braswell, R. Davies, N. Gobron, J. N. Hu, Y. F. Jin, R. A. Kahn, Y. Knyazikhin, N. Loeb, J. P. Muller, et al. (2005), The value of multiangle measurements for retrieving structurally and radiatively consistent properties of clouds, aerosols, and surfaces, *Remote Sens. Environ.*, *97*, 495–518.

Durant, A. J., W. I. Rose, A. M. Sarna-Wojcicki, S. Carey, and A. C. M. Volentik (2009), Hydrometeor-enhanced tephra sedimentation: Constraints from the 18 May 1980 eruption of Mount St. Helens (USA); *J. Geophys. Res.*, *114*, B03204, doi:10.1029/2008JB005756.

Filizzola, C., T. Lacava, F. Marchese, N. Pergola, I. Scaffidi, and V. Tramutoli (2007), Assessing RAT (Robust AVHRR Techniques) performances for volcanic ash cloud detection and monitoring in near real-time: The 2002 eruption of Mt. Etna (Italy), *Remote Sens. Environ.*, *107*, 440–454.

Fiorani, L., F. Colao, A. Palucci (2009), Measurement of Mount Etna plume by CO_2-laser-based lidar, *Opt. Lett.*, *34*, 800–802.

Folch, A., C. Cavazzoni, A. Costa, and G. Macedonio (2008a), An automatic procedure to forecast tephra fallout, *J. Volcanol. Geotherm. Res.*, *177*, 767–777.

Folch, A., O. Jorba, and J. Viramonte (2008b), Volcanic ash forecast—Application to the May 2008 Chaiten eruption, *Nat. Hazards Earth Syst. Sci.*, *94*, 109–117.

Genkova, I., G. Seiz, P. Zuidema, G. Y. Zhao, and L. Di Girolamo (2007), Cloud top height comparisons from ASTER, MISR, and MODIS for trade wind cumuli, *Remote Sens. Environ.*, *107*, 211–222.

Glaze, L. S., L. Wilson, and P. J. Mouginis-Mark (1999), Volcanic eruption plume top topography and heights as determined from photoclinometric analysis of satellite data, *J. Geophys. Res.*, *104*, 2989–3001, doi:10.1029/1998JB900047.

Guffanti, M., G. C. Mayberry, T. J. Casadevall, and R. Wunderman (2009), Volcanic hazards to airports, *Nat. Hazards*, *51*, 287–302.

Holasek, R. E., S. Self, and A. W. Woods (1996), Satellite observations and interpretation of the 1991 Mount Pinatubo eruption plumes, *J. Geophys. Res.*, *101*(B12), 8469–8487, doi:10.1029/96JB01179.

Jiang, X., Y. Liu, B. Yu, and M. Jiang (2007), Comparison of MISR aerosol optical thickness with AERONET measurements in Beijing metropolitan area, *Remote Sens. Environ.*, *107*, 45–53.

Kahn, R., P. Banerjee, D. McDonald, and D. J. Diner (1998), Sensitivity of multiangle imaging to aerosol optical depth and to pure-particle size distribution and composition over ocean, *J. Geophys. Res.*, *103*(D24), 32,195–32,238, doi:10.1029/98JD01752.

Kahn, R., P. Banerjee, and D. McDonald (2001), Sensitivity of multiangle imaging to natural mixtures of aerosols over ocean, *J. Geophys. Res.*, *106*(D16), 18,219–18,238, doi:10.1029/2000JD900497.

Kahn, R. A., W. H. Li, C. Moroney, D. J. Diner, J. V. Martonchik and E. Fishbein (2007), Aerosol source plume physical characteristics from space-based multiangle imaging, *J. Geophys. Res.*, *112*, D11205, doi:10.1029/2006JD007647.

Kalashnikova, O. V., R. Kahn, I. N. Sokolik, and W. H. Li (2005), The ability of multi-angle remote sensing observations to identify and distinguish mineral dust types, part 1: Optical models and retrievals of optically thick plumes, *J. Geophys. Res.*, *110*, D18S14, doi:10.1029/2004JD004550.

Kalashnikova, O. V., and R. Kahn (2006), The ability of multiangle remote sensing observations to identify and distinguish mineral dust types, part 2: Sensitivity data analysis, *J. Geophys. Res.*, *111*, D11207, doi:10.1029/2005JD006756.

Lacasse, C., S. Karlsdottir, G. Larsen, H. Soosalu, W. I. Rose, and G. G. J. Ernst (2004), Weather radar observations of the Hekla 2000 eruption cloud, Iceland, *Bull. Volcanol.*, *5*, 457–473.

Liu, Y., J. A. Sarnat, B. A. Coull, P. Koutrakis, and D. J. Jacob (2004), Validation of multiangle imaging spectroradiometer (MISR) aerosol optical thickness measurements using aerosol robotic network (AERONET) observations over the contiguous United States, *J. Geophys. Res.*, *109*, D06205, doi:10.1029/2003JD003981.

Liu, Y., M. Franklin, R. Kahn, and P. Koutrakis (2007), Using aerosol optical thickness to predict ground-level PM2.5 concentrations in the St. Louis area: A comparison between MISR and MODIS, *Remote Sens. Environ.*, *107*, 33–44.

Martonchik, J. V., D. J. Diner, R. A. Kahn, T. P. Ackerman, M. E. Verstraete, B. Pinty, and H. R. Gordon (1998), Techniques for the retrieval of aerosol properties over land and ocean using multiangle imaging, *IEEE Trans. Geosci. Remote Sens.*, *36*, 1212–1227.

Martonchik, J. V., R. A. Kahn, and D. J. Diner (2009), Retrieval of Aerosol Properties over Land Using MISR Observations. In: A. A. Kokhanovsky and G. de Leeuw, ed., Satellite Aerosol Remote Sensing Over Land. Springer, Berlin.

Mastin, L. G., M. Guffanti, R. Servranckx, P. Webley, S. Barsotti, K. Dean, A. Durant, J. W. Ewert, A. Neri, W. I. Rose, et al. (2009), A multidisciplinary effort to assign realistic source parameters to models of volcanic ash-cloud transport and dispersion during eruptions, *J. Volcanol. Geotherm. Res.*, *186*, 10–21.

Michalakes, J., J. Dudhia, D. Gill, T. Henderson, J. Klemp, W. Skamarock, and W. Wang (2005), The Weather Research and Forecasting model: Software architecture and performance, in *Proc. of the Eleventh ECMWF Workshop on the Use of High Performance Computing in Meteorology*, edited by W. Zwiefhofer and G. Mozdzynski, World Scientific.

Monaco, C., S. Catalano, O. Cocina, G. De Guidia, C. Ferlito, S. Gresta, C. Musumeci, and L. Tortorici (2005), Tectonic control on the eruptive dynamics at Mt. Etna Volcano (Sicily) during the 2001 and 2002–2003 eruptions, *J. Volcanol. Geotherm. Res.*, *144*, 211–233.

Moroney, C., R. Davies, and J. Muller (2002), Operational retrieval of cloud-top heights using MISR data, *IEEE Trans. Geosci. Remote Sens.*, *40*, 1532–1540.

Muller, J. P., A. Mandanayake, C. Moroney, R. Davies, D. J. Diner, and S. Paradise (2002), MISR stereoscopic image matchers: Techniques and results, *IEEE Trans. Geosci. Remote Sens.*, *40*, 1547–1559.

Naud, C., J. P. Muller, and E. E. Clothiaux (2002), Comparison of cloud top heights derived from MISR stereo and MODIS CO_2 slicing, *Geophys. Res. Lett.*, *29*(16), 1795, doi:10.1029/2002GL015460.

Naud, C., J. Muller, M. Haeffelin, Y. Morille, and A. Delaval (2004), Assessment of MISR and MODIS cloud top heights through intercomparison with a back-scattering lidar at SIRTA, *Geophys. Res. Lett.*, *31*, L04114, doi:10.1029/2003GL018976.

Naud, C., J. P. Muller, E. E. Clothiaux, B. A. Baum, and W. P. Menzel (2005), Intercomparison of multiple years of MODIS, MISR, and radar cloud-top heights, *Ann. Geophys.*, *23*, 2415–2424.

Nelson, D. L., Y. Chen, R. A. Kahn, D. J. Diner, and D. Mazzoni (2008), Example applications of the MISR INteractive eXplorer (MINX) software tool to wildfire smoke plume applications, Proc. SPIE Vol. 7089, 708908 (Aug. 27, 2008).

Oppenheimer, C. (1998), Volcanological applications of meteorological satellites, *Int. J. Remote Sens.*, *10*, 2829–2864.

Oppenheimer, C., P. Francis, and I. M. Watson (1998), Advanced Visible and Near Infrared Radiometer (AVNIR) observations of Mount Etna's aerosol plume, *Int. J. Remote Sens.*, *19*(15), 2823–2828.

Pappalardo, G., A. Amodeo, L. Mona, M. Pandolfi, N. Pergola, and V. Cuomo (2004), Raman lidar observations of aerosol emitted during the 2002 Etna eruption. *Geophys. Res. Lett.*, *31*, L05120, doi:10.1029/2003GL019073.

Patanè, D., E. Privitera, S. Gresta, A. Akinci, S. Alparone, G. Barberi, L. Chiaraluce, O. Cocina, S. D'Amico, P. De Gori, et al. (2003), Seismological constraints for the dike emplacement of July–August 2001 lateral eruption at Mt. Etna volcano, Italy, *Ann. Geophys.*, *46*, 599–608.

Peterson, R. A., and K. G. Dean (2008), Forecasting exposure to volcanic ash based on ash dispersion modeling, *J. Volcanol. Geotherm. Res.*, *170*, 230–246.

Prata, A. J., and I. F. Grant (2001), Retrieval of microphysical and morphological properties of volcanic ash plumes from satellite data: Application to Mt. Ruapehu, New Zealand., *Q. J. R. Meteorol. Soc.*, *127*(576B), 2153–2179.

Prata, F., G. Bluth, B. Rose, D. Schneider, and A. Tupper (2001), Comments on "failures in detecting volcanic ash from a satellite-based technique, " *Remote Sens. Environ.*, *78*, 341–346.

Prata, A. J. (2009), Satellite detection of hazardous volcanic clouds and the risk to global air traffic, *Nat. Hazards*, *51*, 303–324.

Pyle, D. M. (1989), The thickness, volume and grain size of tephra fall deposits, *Bull. Volcanol.*, *51*, 1–15.

Pyle, D. M. (2000), Sizes of volcanic eruptions, in *Encyclopedia of Volcanoes*, edited by H. Sigurdsson et al., pp. 263–269, Academic Press, London, UK.

Remitti, M., S. Pugnaghi, and S. Teggi (2006), Mt. Etna aerosol optical thickness from MIVIS images, *Ann. Geophys.*, *49*, 143–151.

Richards, M. S., S. A. Ackerman, M. J. Pavolonis, W. F. Feltz, and A. Tupper (2006), Volcanic ash cloud heights using the MODIS CO_2 slicing algorithm, Conference on Aviation, Range, and Aerospace Meteorology, 12th, Atlanta, Ga, 29 January to 2 February 2006.

Rose, W. I. (1993), Comment on another look at the calculation of fallout tempura volumes, *Bull. Volcanol.*, *55*, 372–374.

Rose, W. I., G. J. S. Bluth, and G. G. J. Ernst (2000), Integrating retrievals of volcanic cloud characteristics from satellite remote sensors: A summary, *Philos. Trans. R. Soc. Lond. Ser. A, Math. Phys. Sci.*, *358*, 1585–1606.

Rose, W. I., G. J. S. Bluth, D. J. Schneider, G. G. J. Ernst, C. M. Riley, L. J. Henderson, and R. J. McGimsey (2001), Observations of volcanic clouds in their first few days of atmospheric residence: The 1992 eruptions of Crater Peak, Mount Spurr Volcano, Alaska, *J. Geol.*, *109*, 677–694.

Sassen, K., J. Zhu, P. Webley, K. Dean, and P. Cobb (2007), Volcanic ash plume identification using polarization lidar: Augustine eruption, Alaska, *Geophys. Res. Lett.*, *34*, L08803, doi:10.1029/2006GL027237.

Sawada, Y. (1987), Study on analysis of volcanic eruptions based on eruption cloud image data obtained by the Geostationary Meteorological Satellite (GMS), Tech. Rep. 22, 335 pp., Meteorol. Res. Inst., Tsukuba, Japan.

Scollo, S., P. Del Carlo, and M. Coltelli (2007), Tephra fallout of 2001 Etna flank eruption: Analysis of the deposit and plume dispersion, *J. Volcanol. Geotherm. Res.*, *160*, 147–164.

Scollo, S., A. Folch, and A. Costa (2008a), A parametric and comparative study on different tephra fallout models, *J. Volcanol. Geotherm. Res.*, *176*, 199–211.

Scollo, S., S. Tarantola, C. Bonadonna, M. Coltelli, and A. Saltelli (2008b), Sensitivity analysis and uncertainty estimation for tephra dispersal models, *J. Geophys. Res.*, *113*, B06202, doi:10.1029/2006JB004864.

Scollo, S., M. Prestifilippo, G. Spata, M. D'Agostino, and M. Coltelli (2009), Forecasting and Monitoring Etna Volcanic Plumes, *Nat. Hazards Earth Syst. Sci.*, *9*, 1573–1585.

Skamarock, W., J. Klemp, J. Dudhia, D. Gill, D. Barker, W. Wang, and J. Powers (2005), A description of the Advanced Research WRF Version 2, Tech note tn-468+str, NCAR. (Available at http://www.wrf-model.org)

Solomon, F., F. Giorgi, and C. Liousse (2006), Aerosol modelling for regional climate studies: Application to anthropogenic particles and evaluation over a European/African domain, *Tellus Ser. B-Chem. Phys. Meteorol.*, *58*, 51–72.

Spinetti, C., M. F. Buongiorno, V. Lombardo, and L. Merucci (2003), Aerosol optical thickness of Mt. Etna volcanic plume retrieved by means of the Airborne Multispectral Imaging Spectrometer (MIVIS), *Ann. Geophys.*, *46*(2), 439–449.

Spinetti, C., and M. F. Buongiorno (2007), Volcanic aerosol optical characteristics of Mt. Etna tropospheric plume retrieved by means of airborne multispectral images, *J. Atmos. Sol.-Terr. Phys.*, *69*, 981–994.

Stenchikov, G., N. Lahoti, P. J. Lioy, P. G. Georgopoulos, D. J. Diner, and R. Kahn (2006), Multiscale plume transport from collapse of the World Trade Center on September 11, 2001, *Environ. Fluid Mech.*, *6*, 425–450.

Taddeucci, J., M. Pompilio, and P. Scarlato (2004), Conduit processes during the July–August 2001 explosive activity of Mt. Etna (Italy): Inferences from glass chemistry and crystal size distribution of ash particles, *J. Volcanol. Geotherm. Res.*, *137*, 33–54.

Tupper, A., S. Carn, J. Davey, Y. Kamada, R. Potts, F. Prata, and M. Tokuno (2004), An evaluation of volcanic cloud detection techniques during recent significant eruptions in the western "Ring of Fire, " *Remote Sens. Environ.*, *91*, 27–46.

Tupper, A., and R. Wunderman (2009), Reducing discrepancies in ground and satellite-observed eruption heights, *J. Volcanol. Geotherm. Res.*, *186*, 22–31.

Villani, M. G., L. Mona, A. Maurizi, G. Pappalardo, A. Tiesi, M. Pandolfi, M. D'Isidoro, V. Cuomo, and F. Tampieri (2006), Transport of volcanic aerosol in the troposphere: The case study of the 2002 Etna plume, *J. Geophys. Res.*, *111*, D21102, doi:10.1029/2006JD007126.

Wang, X., et al. (2008), Volcanic dust characterization by EARLINET during Etna's eruptions in 2001–2002, *Atmos. Environ.*, *42*, 893–905.

Watson, I. M., and C. Oppenheimer (2000), Particle size distributions of Mount Etna's aerosol plume constrained by Sun photometry, *J. Geophys. Res.*, *105*(D8), 9823–9829, doi:10.1029/2000JD900042.

Watson, I. M., and C. Oppenheimer (2001), Photometric observations of Mt. Etna's different aerosol plumes, *Atmos. Environ.*, *35*, 3561–3572.

Watt, S. F. L., D. M. Pyle, T. A. Mather, R. S. Martin, and N. E. Matthews (2009), Fallout and distribution of volcanic ash over Argentina following the May 2008 explosive eruption of Chaitén, Chile, *J. Geophys. Res.*, *114*, B04207, doi:10.1029/2008JB006219.

Wen, S., and W. I. Rose (1994), Retrieval of sizes and total masses of particles in volcanic clouds using AVHRR channels 4 and 5, *J. Geophys. Res.*, *99*(D3), 5421–5431, doi:10.1029/93JD03340.

Witham, C. S., M. C. Hort, R. Potts, R. Servranckx, P. Husson, and F. Bonnardot (2007), Comparison of VAAC atmospheric dispersion models using the 1 November 2004 Grimsvotn eruption, *Meteorol. Appl.*, *14*, 27–38.

Zerefos, C., P. Nastos, D. Balis, A. Papayannis, A. Kelepertsis, E. Kannelopoulou, D. Nikolakis, C. Eleftheratos, W. Thomas, and C. Varotsos (2006), A complex study of Etna's volcanic plume from ground-based, in situ and space-borne observations, *Int. J. Remote Sens.*, *27*, 1855–1864.

M. Coltelli and S. Scollo, Istituto Nazionale di Geofisica e Vulcanologia-Sezione Catania, Piazza Roma 2, Catania 95123, Italy. (coltelli@ct.ingv.it; scollo@ct.ingv.it)

A. Folch, Barcelona Supercomputing Center, Nexus II Building, c/ Jordi Girona, 29, 08034 Barcelona, Spain. (arnau.folch@bsc.es)

V. J. Realmuto, Jet Propulsion Laboratory, California Institute of Technology, 4800 Oak Grove Dr., Pasadena, CA 91109, USA. (vincent.j.realmuto@jpl.nasa.gov)